Theor Chem Acc (2003) 110:59–69
DOI 10.1007/s00214-003-0445-3

Theoretical Chemistry Accounts

Feature article

The role of vibronic interactions on intramolecular and intermolecular electron transfer in π-conjugated oligomers

V. Coropceanu[1], **J.M. André**[1,2], **M. Malagoli**[1], **J.L. Brédas**[1]

[1] Department of Chemistry, The University of Arizona, Tucson, AZ 85721-0041, USA
[2] Laboratoire de Chimie Théorique Appliquée, Facultés Universitaires Notre-Dame de la Paix, 5000 Namur, Belgium

Received: 9 February 2003 / Accepted: 1 April 2003 / Published online: 15 August 2003

Abstract. The importance of electron-vibrational coupling for intermolecular and intramolecular electron-transfer processes is discussed on the basis of first-principles correlated quantum-mechanical calculations and of a dynamic vibronic approach. The methodology is illustrated for examples selected from some of our recent work. In all instances, the theoretical results are thoroughly compared to experimental data.

Keywords: Electron transfer – Charge transfer – Mixed-valence compounds – Vibronic interactions

1 Introduction

Electron transfer (ET) plays a fundamental role in biological, physical, and chemical systems. As a result of major advances in experimental and computational techniques, great progress has been achieved in the understanding and control of ET processes. The current state of the art has been described in two recent volumes of *Advances in Chemical Physics* edited by Jortner and Bixon [1] and a five-volume handbook edited by Balzani [2]. Here, we present an overview of our recent work on intramolecular and intermolecular ET in π-conjugated oligomers.

Molecular and polymer organic semiconductors are currently the object of much interest because of their potential applications in (opto)electronic devices such as light-emitting diodes, photovoltaic cells, field-effect transistors, or photorefractive systems [3, 4, 5, 6]. For instance, triphenylamine (TPA, **1**), see Fig. 1, is a prototypical hole-transport material; its derivatives such as *N,N′*-diphenyl- *N,N′* -bis(3-methylphenyl)-(1,1′-biphenyl)-4,4′-diamine (TPD, **2**) are widely used as hole-transport layers [7, 8, 9]. Understanding charge transport in such materials is important for the design of efficient devices; this requires the characterization of charge carrier mobility, whose mechanism involves ET reactions.

In π-conjugated systems, there exists a strong coupling between the geometric and electronic structures that controls the transport properties [10, 11]. Any charge-injection or electronic-excitation process leads to very fast (subpicosecond) geometry relaxations, which in turn modify the electronic structure [10, 11, 12]. When the charge carriers remain on individual molecules or chain segments for a time sufficiently long that the nuclei relax to the optimal geometry of the charged state, the transport regime corresponds to hopping; this is the situation usually found in π-conjugated materials around room temperature. At the microscopic level, the charge-transport mechanism can then be described as a self-exchange ET from a charged, relaxed chain segment (or molecule) to an adjacent neutral segment (molecules). Several models have been proposed to estimate the carrier mobility [13, 14]. At high temperature when the motions of the carriers can be modeled by a sequence of uncorrelated hops, the key parameters that define the mobility are given by

$$\mu = \frac{ea^2}{k_B T} k_{ET} \quad . \tag{1}$$

Here, k_B denotes the Boltzmann constant, T is the temperature, e is the electronic charge, a denotes the spacing between molecules or chain segments, and k_{ET} is the hopping probability per unit time (ET rate).

In the context of semiclassical ET theory and extensions thereof [15, 16, 17, 18, 19], there are two major parameters that determine the self-exchange ET rate and ultimately the charge mobility: the electronic coupling, H_{ab}, (transfer integral) between adjacent molecules/segments, which needs to be maximized; and the reorgani-

Correspondence to: J.L. Brédas
e-mail: jean-luc.bredas@chemistry.gatech.edu

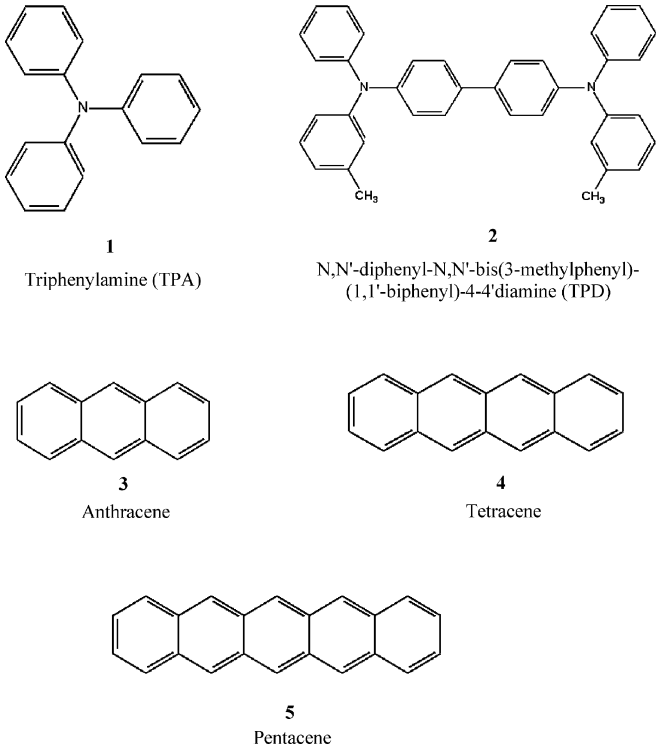

Fig. 1. Chemical formulas of triphenylamine (*TPA*) (**1**), *N,N′*-diphenyl-*N,N′*-bis(3-methyl phenyl)-(1,1′-biphenyl)-4,4′-diamine (*TPD*) (**2**), and oligoacenes (**3**–**5**)

zation energy, λ, which needs to be small for efficient transport. The reorganization energy involves the geometry modifications that occur when electrons are added or removed as well as modifications in the surrounding medium coming from charge polarization. In the high-temperature limit, the rate constant can be cast in an Arrhenius-like form:

$$k_{\mathrm{ET}} = A \exp\left[-\frac{(\lambda - 2H_{\mathrm{ab}})^2}{4\lambda k_{\mathrm{B}} T}\right] = \kappa_{\mathrm{el}} \nu_{\mathrm{n}} \exp\left(-\frac{\Delta G^{\#}}{k_{\mathrm{B}} T}\right) \quad . \tag{2}$$

$\Delta G^{\#}$ is the free energy of activation; the prefactor A can be conveniently expressed as shown in Eq. (2) as the product of the electronic transmission coefficient, κ_{el}, and the nuclear vibration frequency, ν_{n}, that takes the system from reactants to products through the intersection region. In the framework of the Landau–Zener theory [20, 21] κ_{el} is given by [1]

$$\kappa_{\mathrm{el}} = \frac{1 - \exp\left(-\nu_{\mathrm{el}}/2\nu_{\mathrm{n}}\right)}{1 - 0.5\exp\left(-\nu_{\mathrm{el}}/2\nu_{\mathrm{n}}\right)} \quad , \tag{3}$$

where ν_{el} is the electron hopping frequency:

$$\nu_{\mathrm{el}} = \frac{2\pi}{\hbar} H_{\mathrm{ab}}^2 \sqrt{\frac{1}{4\pi\lambda k_{\mathrm{B}} T}} \quad . \tag{4}$$

Taking the inverse of ν_{n} and ν_{el} provides the vibrational and electronic characteristic times, t_{el} and t_{n}, respectively. The two limits $t_{\mathrm{n}} \gg t_{\mathrm{el}}$ ($\nu_{\mathrm{n}} \ll \nu_{\mathrm{el}}$) and $t_{\mathrm{n}} \ll t_{\mathrm{el}}$ ($\nu_{\mathrm{n}} \gg \nu_{\mathrm{el}}$) are referred to as the adiabatic and nonadiabatic regimes.

In an adiabatic limit ($t_{\mathrm{el}} \ll t_{\mathrm{n}}$; $\nu_{\mathrm{el}} \gg \nu_{\mathrm{vib}}$), the electronic states are delocalized over the whole donor–acceptor complex (it is then advantageous to use the double-well delocalized adiabatic representation rather than the localized diabatic representation). The adiabatic ET is understood as the rearrangement of the vibrational degrees of freedom when the system goes from one energy well to the other. For small $\Delta G^{\#}$, the reaction rate constant can approach the nuclear frequency factor. We note that the nuclear frequency ν_{n} can be dominated by a solvent relaxation or an inner-shell vibrational mode. Thus, in the case of strong coupling (adiabatic ET regime), $A = \nu_{\mathrm{n}}$ and the rate constant obeys the standard Arrhenius-type equation:

$$\begin{aligned} k_{\mathrm{ET}} &= \kappa_{\mathrm{el}} \nu_{\mathrm{n}} \exp\left(-\frac{\Delta G^{\#}}{k_{\mathrm{B}} T}\right) \xrightarrow{\kappa_{\mathrm{el}}=1} k_{\mathrm{ET}} \\ &= \nu_{\mathrm{n}} \exp\left(-\frac{\Delta G^{\#}}{k_{\mathrm{B}} T}\right) \quad . \end{aligned} \tag{5}$$

In a nonadiabatic ET reaction ($t_{\mathrm{el}} \gg t_{\mathrm{n}}$; $\nu_{\mathrm{el}} \ll \nu_{\mathrm{n}}$), the vibrational motion is much faster than the electron motion; it goes so fast through the crossing region that the electronic wavefunction does not have enough time to move completely from the donor to the acceptor. Only a small fraction of electronic probability density can reach the donor state (tunneling). In this weak coupling limit, $\kappa_{\mathrm{el}} \ll 1$ and the product $\kappa_{\mathrm{el}}\nu_{\mathrm{n}}$ tends to the hopping frequency ν_{el}. The ET rate is proportional to H_{ab}^2 and also depends on the probability with which the crossing region is reached by the vibrational coordinates (activation energy):

$$\begin{aligned} k_{\mathrm{ET}} &= \kappa_{\mathrm{el}} \nu_{\mathrm{n}} \exp\left(-\frac{\Delta G^{\#}}{k_{\mathrm{B}} T}\right) \xrightarrow{\kappa_{\mathrm{el}}\nu_{\mathrm{n}}=\nu_{\mathrm{el}}} k_{\mathrm{ET}} \\ &= \nu_{\mathrm{el}} \exp\left(-\frac{\Delta G^{\#}}{k_{\mathrm{B}} T}\right) \propto H_{\mathrm{ab}}^2 \exp\left(-\frac{E_{\mathrm{act}}}{k_{\mathrm{B}} T}\right) . \end{aligned} \tag{6}$$

Since the nonadiabatic limit is obtained when the coupling H_{ab} is very small, the splitting at the barrier top is very small.

Equation (6) for nonadiabatic ET can be derived as the classical limit of the quantum mechanical Fermi's golden rule, using time-dependent perturbation theory and assuming that all vibrational modes are classical, $\hbar\omega_i \ll k_{\mathrm{B}} T$. When the reorganization energy λ contains the contributions of both classical modes (λ_0; $\hbar\omega_i \ll k_{\mathrm{B}} T$) and some high-frequency vibrational modes (λ_{h}; $\hbar\omega_{\mathrm{h}} \gg k_{\mathrm{B}} T$), the nonadiabatic ET rate becomes in the context of the Bixon and Jortner model (for details, see the review in Ref. [1]).

$$k_{ET} = \frac{2\pi}{\hbar} H_{ab}^2 \sqrt{\frac{1}{4\pi\lambda_0 k_B T}} \sum_{n=0}^{\infty} \exp(-S_h) \frac{S_h^n}{n!} \times \exp\left[-\frac{(\lambda_0 + n\hbar\omega_h)^2}{4\lambda_0 k_B T}\right] . \quad (7)$$

Here, we assumed that a single effective quantum mode ω_h contributes to λ_h. The Huang–Rhys factor, $S_h = \lambda_h/\hbar\omega_h$, is a measure of the electron-vibrational coupling interaction. The main effect of high-frequency modes is to renormalize the electronic coupling parameter rather than to contribute to the temperature dependence (except at high temperatures). Therefore, in order to achieve a complete understanding of the charge-transport properties, a detailed knowledge of the vibrational modes coupled to the ET process and of the electron-vibration constants is required.

Besides the two limiting cases of adiabatic ($t_{el} \ll t_n$) and nonadiabatic ($t_{el} > > t_n$) reactions, there occur many interesting situations when $t_{el} \approx t_n$. In this case, a vibronic dynamic approach has to be considered, as shown later in the analysis of intramolecular ET and, in particular, of the shape of the lowest intervalence absorption band in triarylamine mixed-valence (MV) systems.

Equations (2), (3), (4), (5), (6), and (7) can be applied to describe both intermolecular and intramolecular ET processes. Figure 2 illustrates how an intermolecular ET process (Fig. 2a) becomes an intramolecular ET process (Fig. 2b) when a bridge is added between the two triarylamine moieties that serve as donor and acceptor sites (M and $M^{+\bullet}$). Molecules where the donor and acceptor sites differ only by their charge (i.e., their oxidation state) are referred to as MV systems. Representative examples of the triarylamine-based MV systems that we have studied are shown in Fig. 3.

The concepts of mixed valency, originally introduced and extensively developed for inorganic systems [22, 23, 24, 25, 26, 27, 28, 29], are increasingly being extended to pure organic compounds [30, 31, 32, 33, 34, 35, 36]. In addition to their relevance to ET processes, MV systems are also the focus of recent research in various related fields owing to their unusual nonlinear optical and magnetic properties and their potential application in molecular electronics and photonics. From a theoretical standpoint, they constitute excellent model systems to test new theoretical approaches.

2 ET processes and reorganization energy

2.1 Determination of reorganization energy from potential surfaces

As stressed in the previous section, the reorganization energy is one of the key quantities that control the ET rate; it is usually expressed as the sum of inner and outer contributions. The inner (intramolecular) reorganization energy arises from the change in equilibrium geometry of the donor and acceptor redox sites consecutive to the gain or loss of electronic charges upon ET. The outer reorganization energy is due to the polarization of the surrounding medium. Owing to the weakness of the van der Waals interactions between organic molecules, the separation of the reorganization energy into intermolecular and intramolecular contributions remains largely valid even in the case of molecular crystals.

The intramolecular reorganization energy for self-exchange consists of two terms corresponding to the geometry relaxation energies upon going from the neutral-state geometry to the charged-state geometry and vice versa (Fig. 4) [37]:

$$\lambda = \lambda_{rel}^{(1)} + \lambda_{rel}^{(2)} , \quad (8)$$

$$\lambda_{rel}^{(1)} = E^{(1)}(M^{+\bullet}) - E^{(0)}(M^{+\bullet}) , \quad (9)$$

$$\lambda_{rel}^{(2)} = E^{(1)}(M) - E^{(0)}(M) . \quad (10)$$

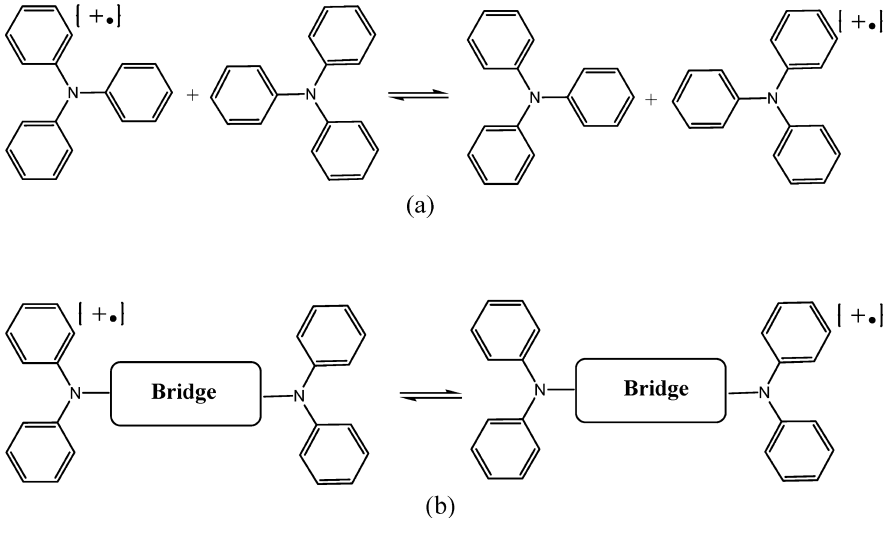

Fig. 2. a Intermolecular and **b** intramolecular electron-transfer processes between TPA moieties

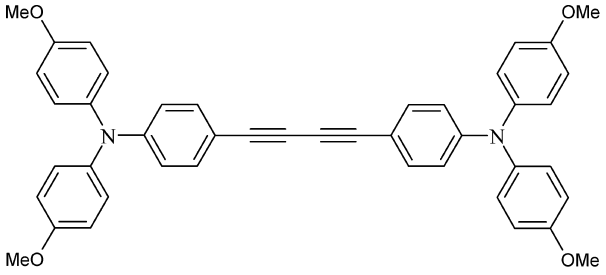

Bis-{4-[N,N-di(4-methoxyphenyl)amino]phenyl}butadiyne **6**

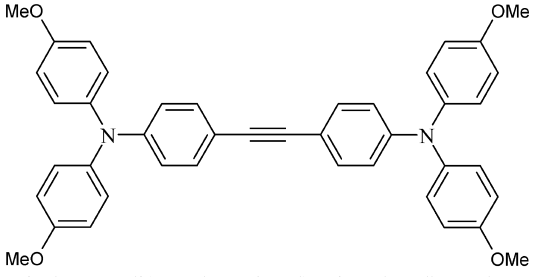

Bis-{4-[N,N-di(4-methoxyphenyl)amino]phenyl}acetylene **7**

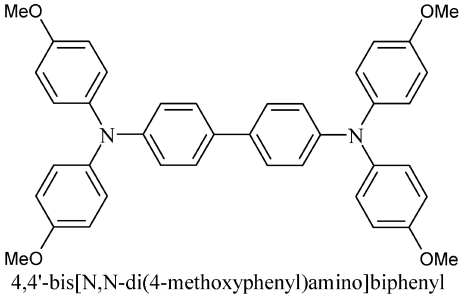

4,4'-bis[N,N-di(4-methoxyphenyl)amino]biphenyl **8**

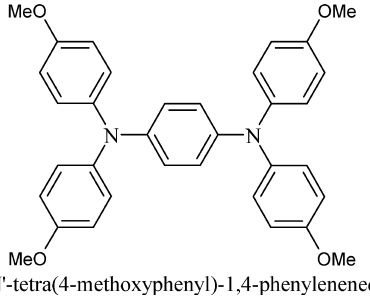

N,N,N',N'-tetra(4-methoxyphenyl)-1,4-phenylenediamine **9**

Fig. 3. Chemical formulas of derivatives **6**–**9**

Here, $E^{(0)}$ (M) and $E^{(0)}$ $(M^{+\bullet})$ are the ground-state energies of the neutral and cation states, respectively. $E^{(1)}$ (M) is the energy of the neutral molecule at the optimal cation geometry; $E^{(1)}$ $(M^{+\bullet})$ is the energy of the cation state at the optimal geometry of the neutral molecule.

2.2 Determination of reorganization energy from frequency analysis

The contributions of each vibrational mode to λ_{rel} can be obtained by expanding the potential energies of the donor and acceptor states in a power series of the normal coordinates. In the harmonic approximation, λ_{rel} can be written as

$$\lambda_{\text{rel}} = \frac{1}{2}\sum_j k_j \Delta Q_j^2 = \sum_j \hbar\omega_j S_j \ . \tag{11}$$

ΔQ_j represents the displacement along normal mode j between the equilibrium positions of the two electronic states of interest; k_j is the corresponding force constant. We note that when both donor and acceptor possess an orbitally nondegenerate ground state, only totally symmetric vibrations contribute to the relaxation energy.

The numerical procedure consists of the following steps. First, the normal-mode coordinates and the force constants are determined. Then, the normal mode displacements ΔQ_j are obtained by projecting the displacements between the equilibrium geometries of the donor and acceptor states onto the normal-mode vectors. Finally, by substituting the calculated quantities into Eq. (11), the total relaxation energy is obtained.

Hereafter, the numerical approaches discussed earlier are applied to the triarylamine and oligoacene systems shown in Fig. 1. The geometry optimizations, normal-mode analysis, and all single-point calculations were performed at the density functional theory (DFT) level with the hybrid B3LYP functionals [38, 39] using the standard 6-31G** basis set. All the calculations were carried out with the Gaussian98 suite of programs [40].

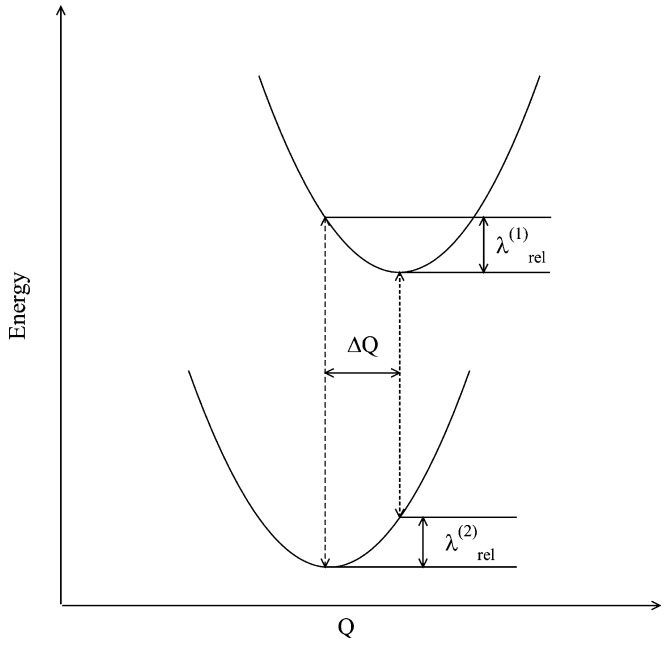

Fig. 4. Typical adiabatic energy surfaces corresponding to the ionization (attachment) process

2.3 Intramolecular reorganization energy: triarylamine derivatives

The optimized geometry for the neutral TPA molecule (**1**) corresponds to an sp^2 hybridization (planar configuration) of the nitrogen atom; the three phenyl groups assume a propeller-like structure, with a torsion angle of 41.70 with respect to the plane defined by the three N–C bonds. The geometrical structure of the radical cation $\mathbf{1}^+$ differs only slightly from the neutral one: the amino group remains planar, the torsion angles of the phenyl groups decrease to 38.9°, and the C–N bond lengths change from 1.42 Å in the neutral molecule to 1.41 Å in the cation [37].

In the case of TPD (**2**), the neutral molecule keeps the geometrical characteristics of its components; the TPA moieties of neutral TPD exhibit a planar configuration of the N–C bonds and N–C bond lengths of 1.42 Å. The central part has a structure close to that observed in isolated biphenyl. The structure of the positive ion is significantly perturbed upon ionization; while similarity between the central part of the molecule and biphenyl is conserved and the N–C bonds remain in the same plane, a marked asymmetry is observed in the C–N bond lengths as the C–N bond with the central biphenyl segment is significantly shorter than the other two (1.39 versus 1.43 Å) [37].

The results of geometry optimizations indicate that upon ionization, **2** undergoes a reorganization similar to that occurring in biphenyl and significantly different from the one observed in **1**. The relaxation energies $\lambda_{rel}^{(2)}$ and $\lambda_{rel}^{(1)}$ obtained from Eqs. (9) and (10) are 0.06 and 0.06 eV for **1**, 0.15 and 0.14 eV for **2**, and 0.17 and 0.19 eV for biphenyl. This points out the intrinsic difference of the relaxation processes occurring in **1** and **2**. In TPD, it is the large geometry relaxation occurring in the biphenyl core that dominates the reorganization energy and leads to a λ value close to that obtained for the biphenyl molecule.

2.4 Intramolecular reorganization energy: oligoacene derivatives

We have studied oligoacenes containing from three to five rings: anthracene (**3**), tetracene (**4**), and pentacene (**5**). The geometry optimizations indicate that the bond-length modifications upon positive ionization show a consistent trend along the series. Anthracene displays the largest geometry relaxations, with changes in C–C bond lengths of the order of 0.02 Å. This value is reduced to about 0.015 and 0.01 Å in tetracene and pentacene, respectively. The geometry distortions, as well as the changes in atomic charge densities (Mulliken populations), are spread over the entire molecules. This indicates that even for pentacene, the largest oligomer studied here, the molecular size is still smaller than the molecular polaron extension. The theoretical estimates of the relaxation energies $\lambda_{rel}^{(2)}$ and $\lambda_{rel}^{(1)}$ obtained from the adiabatic potential surfaces are 0.068 and 0.069 eV for **3**, 0.056 and 0.057 eV for **4**, and 0.048 and 0.049 eV for **5** [41], leading to total reorganization energies of 0.137, 0.113, and 0.097 eV, respectively, for the three molecules. The dependence of the reorganization energy on the conjugation length is presented in Fig. 5. As observed previously [42], the reorganization energy (electron–phonon coupling) is inversely proportional to the number of atoms along the π-conjugated backbone. In the limit of infinite conjugation length, the reorganization energy converges to a value around 0.025 eV.

In the case of pentacene, the partition of the reorganization energy into the contributions of each vibrational mode is listed in Table 1. The reorganization energy obtained from the normal-mode analysis, $\lambda = 0.1$ eV, is in excellent agreement with the value reported earlier, $\lambda = 0.097$ eV, computed directly from the adiabatic potential-energy surfaces. The main contributions to the relaxation energy come from a few normal modes in the range of 1,200–1,600 cm^{-1}. The same trend is observed in anthracene and tetracene [41, 43]. Note that in all the systems considered here, the relaxation energies $\lambda_{rel}^{(1)}$ and $\lambda_{rel}^{(2)}$ are nearly identical to one another.

2.5 Experimental determination of intramolecular reorganization energy

The vibrational reorganization energy of a single molecule can be estimated experimentally from its gas-phase photoelectron spectrum [44]. The vibrational structure present in an ionization band provides the values of the Huang–Rhys factors, S_j, and of the frequencies of the

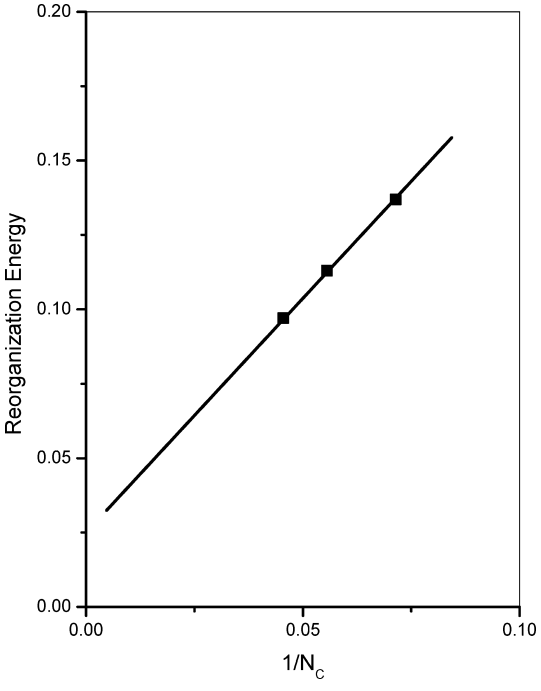

Fig. 5. Dependence of the reorganization energy on the inverse of the number of carbon atoms in anthracene, tetracene, and pentacene

Table 1. Density functional theory (*DFT*) estimates of frequencies, Huang–Rhys factors, S, and reorganization energies $\lambda_{rel}^{(2)}$ and $\lambda_{rel}^{(2)}$ for pentacene

ω/cm^{-1}	S	$\lambda_{rel}^{(1)}/eV$	ω/cm^{-1}	S	$\lambda_{rel}^{(2)}/eV$
263	0.030	0.0010	264	0.031	0.0010
613	0.000	0.0000	616	0.000	0.0000
636	0.000	0.0000	646	0.000	0.0000
765	0.000	0.0001	764	0.000	0.0000
807	0.002	0.0002	799	0.002	0.0002
1,046	0.004	0.0005	1,027	0.004	0.0008
1,200	0.015	0.0022	1,190	0.011	0.0016
1,227	0.043	0.0073	1,218	0.052	0.0078
1,338	0.004	0.0007	1,345	0.000	0.0001
1,425	0.003	0.0006	1,425	0.074	0.0130
1,441	0.097	0.0184	1,447	0.013	0.0024
1,515	0.000	0.0001	1,506	0.002	0.0003
1,560	0.059	0.0118	1,569	0.098	0.0190
1,590	0.033	0.0072	1,590	0.011	0.0021
3,192	0.000	0.0001	3,165	0.000	0.0000
3,196	0.000	0.0002	3,171	0.000	0.0000
3,202	0.000	0.0002	3,175	0.001	0.0002
3,224	0.001	0.0001	3,200	0.000	0.0001
Total		0.0506	Total		0.0488

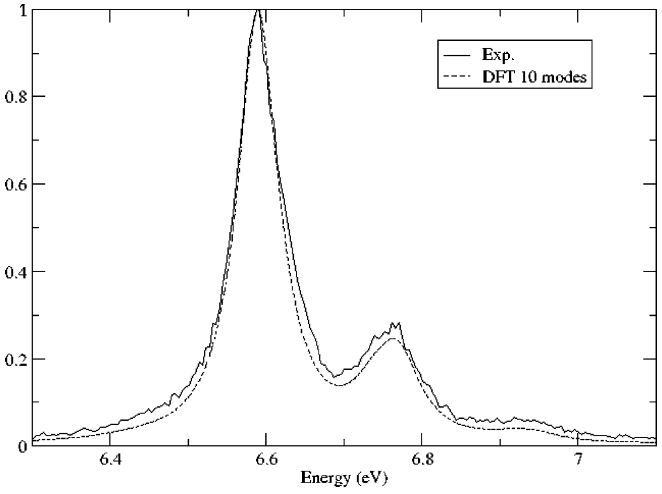

Fig. 6. Density functional theory (*DFT*) simulation of the first ionization peak of the UV photoelectron spectroscopy spectrum of pentacene. The ten vibrational modes of Table 1 with the largest Huang–Rhys factors were used for the simulation. The frequencies were scaled by a factor of 0.9613. The transition intensities were convoluted using Lorentzian functions with a full width at half maximum of 0.06 eV

coupled modes. Experimental results of this type can also be derived from other spectroscopies, in particular resonance Raman [45], or from the temperature dependence of the ET rate constants [46]; however, in such methods, it is necessary to separate the inner contribution from the solvent reorganization energy. Thus, gas-phase UV photoelectron spectroscopy (UPS) has the merit to provide directly the inner contribution.

We have recently used gas-phase UPS to estimate the reorganization energies of anthracene, tetracene, and pentacene [41, 47]. The experimental results confirm that the reorganization process in all three systems is dominated by the interaction with rather high-frequency modes, in agreement with the theoretical results of Table 1. The numerical simulation of the first ionization band of pentacene obtained from the linear vibronic model and using the data from Table 1 is reported in Fig. 6 together with the experimental UPS spectrum. The agreement between theory and experiment is excellent.

It is interesting to note that λ is directly related to such quantities as the polaron binding energy ($E_{pol} = \lambda/2$) and the dimensionless electron–phonon parameter $\lambda_{e\text{-}ph}$ [$\lambda_{e\text{-}ph} = \lambda N(E_F)$, where $N(E_F)$ is the density of states at the Fermi level] [41, 42]. The electron–phonon parameter is a key value in the conventional theory of superconductivity. Therefore, the results discussed above are of particular importance in the development of adequate polaron models to understand superconductivity and charge transport in organic molecular systems.

3 Intramolecular ET: MV systems

3.1 Vibronic model

The properties of MV systems depend strongly on the extent of electronic interaction between the redox sites. In accordance with the common classification, MV systems are divided into three classes [48]: class I, complete valence trapping (negligible electronic coupling between the two redox sites); class II, valence trapping (weak electronic coupling); and class III, delocalized valency (strong electronic coupling).

Organic MV systems are of interest because many of them, in particular those represented in Fig. 3, display a significant electronic coupling and are thus appropriate for the investigation of adiabatic ET processes. As a consequence of the strong electronic interactions, the ET rate is too fast to be measured directly by experimental techniques such as electron spin resonance or NMR; however, it can be accessed from optical data since an important feature of the electronic spectrum of MV systems is the appearance of an absorption band in the visible or near-IR region. This band, referred to as the intervalence charge-transfer (IV-CT) band results from transitions within the electron-vibrational manifold generated by the electronic interaction between the redox sites. This band can be analyzed to provide the values of the two ET parameters: the electronic coupling H_{ab} and the reorganization energy λ.

The first vibronic coupling model that is applicable to classes II and III of MV systems is the Piepho, Krausz, and Schatz (PKS) model [49, 50]. It is a two-site one-mode model in which only the donor and acceptor states are considered. The single vibrational mode of the PKS model represents the out-of-phase (antisymmetric) linear combination of the breathing modes localized on the donor and acceptor sites. Ondrechen and coworkers [51, 52] have extended this model by explicitly taking into account the role of the bridge ligand and of its vibrational modes; in a more advanced model, Piepho [53, 54] has stressed the role of multicenter vibrations that gov-

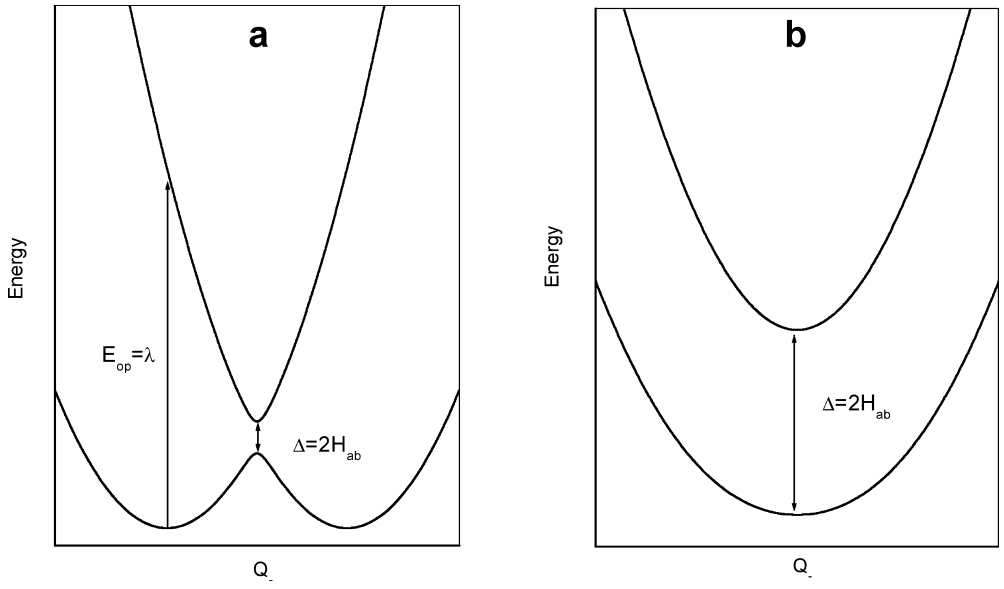

Fig. 7. Typical adiabatic energy surfaces in the case of diagonal vibronic coupling: **a** broken-symmetry situation (class II); **b** symmetric situation (class III)

ern the donor–acceptor distance. We note that the fact that the interaction with symmetric vibrations could be a major source of band broadening for strongly delocalized MV systems was predicted by Hush over 20 years ago [55].

In the case of $\mathbf{6}^+$, we have previously shown that the PKS model reproduces the major features of the CT band, i.e., its position, intensity, width, and asymmetry. However, some disagreements subsist. For instance, the smooth decrease observed experimentally on the high-energy side of the CT band is not correctly reproduced. More recently, we obtained a better description by including the symmetric vibrations into the model. For that purpose, we employed a simple two-mode model using a set of two molecular normal coordinates that only contain the contributions of one symmetric vibration, Q_+, and one antisymmetric vibration, Q_-. In the delocalized electronic basis

$$\Psi_{\pm} = \frac{1}{\sqrt{2}}(\Psi_a \pm \Psi_b) \ , \tag{12}$$

where Ψ_a and Ψ_b are the wavefunctions of the diabatic states corresponding to the two possible valence structures $M_a^{+\bullet}$–bridge– M_b or M_a–bridge– $M_b^{+\bullet}$, the system is described by the following vibronic Hamiltonian:

$$H_{vib} = \begin{pmatrix} T_{Q_+} + T_{Q_-} + \frac{1}{2}(k_- Q_-^2 + k_+ Q_+^2) & \ell_- Q_- \\ \ell_- Q_- & T_{Q_+} + T_{Q_-} + \frac{1}{2}(k_- Q_-^2 + k_+ Q_+^2) + \Delta + \ell_+ Q_+ \end{pmatrix} . \tag{13}$$

Here, k_+ and k_- are the force constants and we assume that they are identical in both electronic states Ψ_+ and Ψ_-; ℓ_+ and ℓ_- are the linear vibronic constants. In Eq. (13), the energy difference $\Delta = \varepsilon_+ - \varepsilon_-$ between the molecular electronic states Ψ_+ and Ψ_- is related to the electronic coupling constant $H_{ab} = \Delta/2$. It is important to mention that in contrast to the conventional Hush model [17, 18] where H_{ab} is assumed constant, the effective electronic coupling in the present model depends on the coordinates of the symmetric vibration. In Eq. (2), Δ is defined at the transition state where H_{ab} is maximal.

The eigenvalues and eigenfunctions of the vibronic matrix H_{vib} (that take into account the nuclear kinetic energy) form the complete solution of the dynamic vibronic problem [26].

3.2 Adiabatic solutions

We first consider the static (adiabatic) solutions of the problem, i.e., the solutions obtained in the framework of the Born–Oppenheimer approximation from the electronic Hamiltonian only, without considering the nuclear kinetic energy. The resulting adiabatic potential surfaces are plotted in Fig. 7 when only the off-diagonal vibronic coupling is operative ($\ell_- \neq 0$ and $\ell_+ = 0$). Provided $\ell_-^2/k_- > H_{ab}$ (class II), the vibronic mixing of the electronic states leads to a pseudo-Jahn–Teller instability of the reference symmetric geometry; the lower surface of the adiabatic potential exhibits two equivalent minima corresponding to two broken-symmetry states (Fig. 7a). Each of these minima corresponds to the situation where the system is mainly localized on one of the valence structures, $M_a^{+\bullet}$–bridge–M_b or M_a–bridge–$M_b^{+\bullet}$. Thus, the vibration Q_- corresponds to the reaction coordinate of the standard one-dimensional

self-exchange ET theory. In both cases of intermolecular and intramolecular ET, Q_- can be considered as an antisymmetric linear combination of symmetric modes localized on the donor and acceptor sites. λ is related to ℓ_- by

$$\lambda = 2\ell_-^2/k_- \ . \tag{14}$$

It can be shown that Eq. (14) is equivalent to the definitions given by Eqs. (8), (9), (10), and (11) if the vibronic interaction of the donor site and of the acceptor sites is limited to a single vibration. It is important to note that, despite an apparent similarity, the origin of the reorganization energies (Eqs. 11, 14) in intermolecular and intramolecular ET processes is different: In the first case, as already underlined, only the totally symmetric vibrations contribute to λ; in the second case, λ is determined by the antisymmetric modes (now Q_- is an intramolecular vibrational mode).

When $\ell_-^2/k_- \leq H_{ab}$ (class III), the lower surface possesses only one minimum (Fig. 7b). The symmetric equilibrium structure is then stable with respect to the antisymmetric vibrations.

Owing to the Franck–Condon principle, the optical band corresponds to a vertical transition from a minimum in the lower surface to the upper surface, as shown in Fig. 7. In the case of weakly coupled systems ($H_{ab} < \ell_-^2/k_-$ or equivalently $\Delta < \lambda$), the maximum of the CT optical band, E_{op}, is equal to λ:

$$E_{op} = h\nu_{max} = \lambda \ . \tag{15}$$

The CT band is Gaussian-shaped with a full width at half maximum, $\nu_{1/2}$, given at high temperature by the Hush relation:

$$\nu_{1/2}{}^2 = 16\lambda k_B T \ln 2 \ . \tag{16}$$

The intensity of the CT transition is related to the electronic coupling H_{ab} by the expression

$$H_{ab} = \frac{0.0206}{R}\left(\nu_{max}\varepsilon_{max}\nu_{1/2}\right)^{1/2} \ , \tag{17}$$

where H_{ab}, ν_{max}, and $\nu_{1/2}$ are given in reciprocal centimeters. R (in angstroms) is the effective separation distance between the donor and the acceptor sites (diabatic states); ε (per mole per centimeter) denotes the molar extinction coefficient. Note, that while the parameters ε, ν_{max}, and $\nu_{1/2}$ are accessible from optical measurements, the diabatic transfer distance R cannot in principle be directly measured. Much later after Hush's seminal work, Cave and Newton [56] developed a prescription on how to obtain R using experimental and/or theoretical data (see Sect. 3.4).

In the case of strongly coupled MV systems, $\Delta > \lambda$ (class III), the energy of the intervalence transition becomes a direct measure of the electronic coupling:

$$E_{op} = \Delta = 2H_{ab} \ . \tag{18}$$

The reorganization energy L related to the symmetric mode can be obtained from the displacement of the upper adiabatic surface with respect to the ground adiabatic surface at the symmetric geometry configuration $Q_- = 0$. This displacement is due to the sensitivity of the molecular geometry to the perturbation of the electron distribution occurring during the optical excitation. Thus, the energy of the intervalence transition can be written as

$$\begin{aligned} E_{op} &= \Delta = \Delta_0 + L \ , \\ L &= \frac{k_+(\delta Q_+)^2}{2} \ , \end{aligned} \tag{19}$$

where Δ_0 is the energy difference between the ground and excited states each at their own equilibrium positions and $\delta Q_+ = \ell_+/k_+$ is the displacement of the two adiabatic potential curves. In conventional molecular spectroscopy, L is usually referred to as the relaxation energy. Note, however, that both λ and L bear the same physical meaning (i.e., they correspond to vibrational reorganization energy); they are distinguished only by the relevant vibrational mode (i.e., antisymmetric for λ and symmetric for L). If the interaction with symmetric vibrations is strong, the shape of the CT band can be broad even in the case of class III systems.

3.3 Electronic coupling

The electronic coupling parameter of systems $\mathbf{6}^+$–$\mathbf{9}^+$ was evaluated in three ways: from excited-state calculations at the TD-DFT level [57]; directly from DFT calculations; and by means of Koopmans' theorem (KT) [58]. As seen from Fig. 7, in class II compounds, the coupling parameter Δ should be calculated at the transition-state structure rather than at the equilibrium geometry. In order to locate the symmetric geometry configuration, the optimization of the radical-cation states was also performed with symmetry constraints, i.e., keeping the two halves of the molecule identical. In addition, to rule out a possible artifact of the DFT geometry optimizations, as a crosscheck, all the electronic calculations were also carried out at the neutral molecular geometry.

The TD-DFT energy and the transition dipole moment of the first excited state of systems $\mathbf{6}^+$–$\mathbf{9}^+$ were obtained at the B3LYP/6-31G** level. The results indicate that the first optical band is due to a single electronic transition to an excited state well separated from any other state. For all four systems, the main configuration interaction contribution to the state in question is described by the HOMO$\beta \rightarrow$ LUMOβ one-electron transition (if we were to use the labels of the levels in the neutral state, this would correspond to the HOMO-1 $\rightarrow$ HOMO excitation).

In the case of open-shell molecules, the DFT method can be used directly to calculate the lowest state of any symmetry. Since in our case the two states of interest, Ψ_+ and Ψ_-, are of different symmetry, it is possible to estimate the electronic coupling parameter, $\Delta = \varepsilon_+ - \varepsilon_-$, by applying directly the DFT method to these two states. For all systems, the DFT estimates are smaller than the TD-DFT values.

Currently, the evaluation of the electronic coupling is frequently based on the simple application of KT. In this approach, the magnitude of Δ is approximated by the energy difference between the delocalized active molecular orbitals taken from a selected electronic configuration. In our calculations, Δ was estimated from the difference in the energies of the HOMO and HOMO-1 levels derived from the closed-shell configuration of the neutral molecule. Both Hartree–Fock-type (HF) and Kohn–Sham-type (KS) orbitals were used. The comparison of the data in Table 2 indicates that the KT-KS values are somewhat larger than the DFT values but remain significantly lower than the TD-DFT estimates. In contrast, the KT-HF values are comparable with the TD-DFT results. The Δ parameters were calculated at the KT-AM1 level using the AM1-optimized geometry of the neutral species. Here, for the sake of a better comparison, we performed the KT-AM1 calculations at the same DFT-optimized geometry as for the KT-KS and KT-HF calculations. The KT-AM1 results provide lower Δ values than the other calculations.

In order to illustrate the influence of the choice of geometry, we calculated the ratio $\eta = \Delta$ (at cation geometry)/Δ (at neutral geometry). The results are also given in Table 2. It appears that the TD-DFT values are less sensitive to the choice of geometry than the KT estimates; the largest TD-DFT value for η is obtained for compound $\mathbf{7}^+$, $\eta = 1.18$, and is to be compared to $\eta = 1.39$, 1.41, and 1.49 obtained for the same compound from the KT-KS, KT-HF, and KT-AM1 calculations, respectively.

Thus, the electronic-structure calculations point toward a strong electronic coupling in triarylamine-based MV systems. This coupling is sufficiently strong even in the case of system $\mathbf{6}^+$, where a long bridge separates the TPA moieties, that the ET reaction in this molecule also takes place in the adiabatic regime.

It is worth mentioning here that, owing to problems inherent to DFT exchange–correlation functionals [59], DFT calculations can sometimes result in an overstabilization of delocalized states. On the other hand, it was shown that conventional HF methods based on single-configuration wavefunctions fail for the radical-cation state of the systems considered here [34]. Therefore, calculations at a multiconfigurational level are generally required.

3.4 ET distance

The Hush model remains the method of choice for the determination of the electronic coupling because of its simplicity and ease of application. Equation (17) was initially derived at the perturbation limit of weak electronic coupling and for Gaussian-shaped bands. A more general formulation of this equation applicable for arbitrary band shapes is [60]

$$H_{ab} = \frac{\mu_{12}}{eR} \nu_{max} \quad . \tag{20}$$

Here, μ_{12} is the IV-CT transition dipole moment. According to Cave and Newton [56], the ET distance, R, can be estimated as

$$eR = \sqrt{\Delta\mu_{12}^2 + 4\mu_{12}^2} \quad . \tag{21}$$

$\Delta\mu_{12}$ is the difference between the dipole moments corresponding to the minima of the lower adiabatic potential surface. In this approach, $\Delta\mu_{12}$ is obtained as twice the ground-state dipole moment, provided the origin of the coordinate system is located on the molecular center of symmetry [61, 62]. Alternatively, R can be estimated from the calculations of the transition dipole moment $\mu_\pm$ for the electronic $\Psi_+ \rightarrow \Psi_-$ transition:

$$eR = 2\mu_\pm \tag{22}$$

The values of R obtained from TD-DFT estimates of $\mu_\pm$ are collected in Table 3. They indicate that the ET distance is much smaller than the nitrogen–nitrogen

Table 2. Absolute values of Δ (cm^{-1}) for systems $\mathbf{6}^+$–$\mathbf{9}^+$ obtained from TD-DFT, DFT, and Koopmans' theorem (*KT*) calculations using the geometry of the radical-cation state and, in *parentheses*, of the neutral state

Method	System			
	$\mathbf{9}^+$	$\mathbf{8}^+$	$\mathbf{7}^+$	$\mathbf{6}^+$
TD-DFT	9,250 (7,940)	6,920 (5,860)	6,550 (5,900)	6,040 (5,480)
η	1.16	1.18	1.11	1.10
DFT	7280	4290	3950	3640
KT/HF	9,930 (7,460)	7,080 (5,090)	6,570 (5,140)	5,390 (4,290)
η	1.33	1.39	1.28	1.26
KT/DFT	7,720 (5,720)	4,660 (3,310)	4,550 (3,540)	3,970 (3,160)
η	1.34	1.41	1.29	1.26
KT-AM1-RHF	6,850 (4,740)	4,190 (2,820)	3,460 (2,510)	2,650 (1,970)
η	1.45	1.49	1.38	1.34

Table 3. Electron transfer distances, R, for systems $\mathbf{6}^+$ –$\mathbf{9}^+$ obtained from TD-DFT calculations. The nitrogen–nitrogen distances are taken from the DFT-optimized geometries of the radical-cation state

	$\mathbf{6}^+$	$\mathbf{7}^+$	$\mathbf{8}^+$	$\mathbf{9}^+$
R (Å)	7.72	6.89	6.05	4.22
R_{NN} (Å)	15.06	12.49	9.95	5.62

distance (that could in principle be considered as the geometric separation of the two localized sites).

The application of Eq. (18) is complicated by the fact that the value of the dipole moment $\Delta\mu_{12}$ strongly depends on the method used for geometry optimization. For example, the DFT calculation results in a nearly symmetric configuration close to that obtained with symmetry constraints and thus yields a very small value of R; for instance, $R = 5.2$ Å for system $\mathbf{7}^+$. This value is much smaller than the estimate based on TD-DFT calculations. In contrast to DFT, the HF optimizations result in an asymmetric geometry with large dipole moments. For system $\mathbf{7}^+$, R calculated at the ab initio unrestricted HF/6-31G** level is 11.7 Å. This value is only slightly smaller than the nitrogen–nitrogen distance of 12.5 Å, and is probably overestimated. We note that the ab initio unrestricted HF calculations suffer from a high amount of spin contamination (e.g., for system $\mathbf{7}^+$ at the unrestricted HF/6-31G** level, $< S^2 > = 3.1$), which strongly questions their reliability.

3.5 Shape of IV-CT bands

In an MV system, the shape of the CT band is an important characteristic of the extent of valence delocalization. Systems $\mathbf{6}^+$–$\mathbf{9}^+$ exhibit a rather intense CT transition. Using the experimental values for the transition dipole moments, the oscillator strengths of the CT transitions are estimated to be 0.15, 0.39, 0.40, and 0.38, respectively. For comparison, the oscillator strength of the Creutz–Taube ion, $[(NH_3)_5Ru$–pyrazine–$Ru(NH_3)_5]^{5+}$ [63], which is considered as a class III system, is about 0.03. Thus, such intensities are an experimental indication that the electronic coupling in these systems is strong. In addition, the bands in the triarylamine systems are significantly broader than in the ruthenium compound; the implication is that the vibronic interactions are also very strong in these systems.

The dynamic vibronic problem for $\mathbf{6}^+$– $\mathbf{9}^+$ was solved in the framework of the numerical procedure presented previously. The resulting eigenfunctions and eigenvalues were used to simulate the CT band. We exploited a basis set truncated to 60 vibrational quanta; we have verified that a further increase in the basis set does not change the profile of the calculated bands. The reorganization energy parameters and the electronic coupling constants were obtained by fitting the position and shape of the theoretical IV-CT bands to the experimental spectra.

The simulations of the shape of the IV-CT band indicate a broken-symmetry effect for $\mathbf{6}^+$ and $\mathbf{7}^+$; thus, these systems can be classified as class II systems. Although it is not possible to draw a definite conclusion about the ratio λ/Δ for $\mathbf{8}^+$ and $\mathbf{9}^+$, the simulations based on the two-mode model reveal that the reorganization energy is smaller or at least does not significantly exceed the electronic coupling parameter; thus, $\mathbf{8}^+$ and $\mathbf{9}^+$ can be classified as borderline between class II and class III systems.

The electronic coupling parameters Δ obtained from the fitting, 9,680 cm^{-1} ($\mathbf{9}^+$), 6,200 cm^{-1} ($\mathbf{8}^+$), 5,100 cm^{-1} ($\mathbf{7}^+$), and 3,300 cm^{-1} ($\mathbf{6}^+$), reveal that TD-DFT provides reliable values in the case of strong electron delocalization but overestimates the electronic coupling of large π-conjugated MV systems; in the case of $\mathbf{6}^+$, which has the longest central bridge, the TD-DFT estimate is about twice as large as that obtained from the dynamic vibronic simulations.

The numerical simulations reveal that the band shape results from a subtle balance between the vibronic interactions with symmetric and antisymmetric modes. The shape of the CT band in $\mathbf{9}^+$ (Fig. 8) is completely dominated by the interaction with the symmetric mode; the same trend is observed for system $\mathbf{8}^+$. In systems $\mathbf{6}^+$ and $\mathbf{7}^+$, the roles of the symmetric and antisymmetric modes are reversed with respect to $\mathbf{8}^+$ and $\mathbf{9}^+$. These results fully support Hush's prediction of the dominant role of symmetric vibrations in determining the band shape in delocalized MV systems.

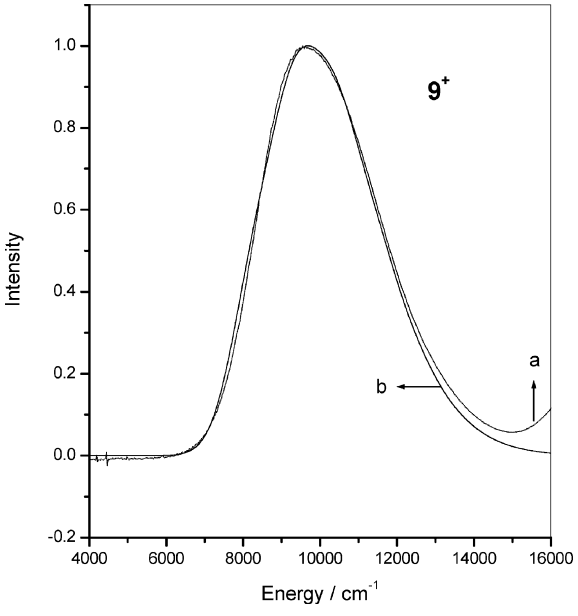

Fig. 8. Calculated absorption profiles of $\mathbf{9}^+$ for the following sets of parameters: (*a*) experimental absorption spectrum taken from Ref. [35]; (*b*) $\Delta = 9{,}680$ cm^{-1}, $\lambda = 6{,}500$ cm^{-1}, $L = 1{,}673$ cm^{-1}, $\hbar\omega_+ = 1{,}050$ cm^{-1}, and $\hbar\omega_- = 500$

4 Synopsis

In this contribution, we have reviewed the parameters of importance in the study of intramolecular and intermolecular ET processes. The various approaches have been illustrated in the case of π-conjugated oligomers corresponding to oligoacenes and triarylamine MV compounds. The interplay of symmetric and antisymmetric vibrations on the ET processes has been highlighted.

Acknowledgements. The work at Arizona has been partly supported by the National Science Foundation (through the STC for Materials and Devices for Information Technology—DMR-0120967—and through CHE-0078819), the Office of Naval Research, and the IBM Shared University Research program. J.M.A. and J.L.B. acknowledge support from the Belgian Federal Government Office for Scientific, Technical and Cultural Affairs: Interuniversity Attraction Pole Program on "Supramolecular chemistry and supramolecular catalysis" (IUAP 5-03).

References

1. Bixon M, Jortner J (eds) (1999) Electron transfer: From Isolated molecules to biomolecules. Advances in chemical physics, vols 106–107. Wiley, New York
2. Balzani V (ed) (2001) Electron transfer in chemistry, vols 1–5. Wiley-VCH, Weinheim
3. (a) Sheats JR, Antoniadis H, Hueschen M, Leonard W, Miller J, Moon R, Roitman D, Stocking A (1996) Science 273:884; (b) Friend RH, Gymer RW, Holmes AB, Burroughes JH, Marks RN, Taliani C, Bradley DDC, dos Santos DA, Brédas JL, Lögdlund M, Salaneck WR (1999) Nature 397:121
4. Yu G, Gao J, Hummelen JC, Wudl F, Heeger AJ (1995) Science 270:1789
5. Bulovic V, Gu G, Burrows PE, Forrest SR, Thompson ME (1996) Nature 380:29
6. Huitema HEA, Gelinck GH, van der Putten JBPH, Kuijk KE, Hart CM, Cantatore E, de Leeuw DM (2002) Adv Mater 14:1201
7. Tamoto N, Adachi C, Nagai K (1997) Chem Mater 9:1077
8. Bellmann E, Shaheen SE, Thayumanavan S, Barlow S, Grubbs RH, Marder SR, Kippelen B, Peyghambarian N (1998) Chem Mater 10:1668
9. Bellmann E, Shaheen SE, Grubbs RH, Marder SR, Kippelen B, Peyghambarian N (1999) Chem Mater 11:399
10. Su WP, Schrieffer JR, Heeger AJ (1979) Phys Rev Lett 42:1698
11. Brédas JL, Street GB (1985) Acc Chem Res 18:209
12. Salaneck WR, Friend RH, Brédas JL (1999) Phys Rep 319:231
13. Kao KC, Hwang W (1981) Electrical transport in solids. Pergamon, Oxford, p 27
14. Pope M, Swenberg CE (1999) Electronic processes in organic crystals and polymers, 2nd edn. Oxford University Press, New York, p 356
15. Marcus RA (1960) Discuss Faraday Soc 29:21
16. Marcus RA, Sutin N (1986) Comments Inorg Chem 5:119
17. Hush NS (1967) Prog Inorg Chem 8:391
18. Hush NS (1985) Coord Chem Rev 64:135
19. DeVault D (1984) Quantum mechanical tunneling in biological systems. Cambridge University Press, Cambridge
20. Landau LD (1932) Phys Z Sowjetunion 1:88
21. Zener C (1932) Proc R Soc Lond Ser 137:696
22. Barbara PF, Meyer TJ, Ratner MA (1996) J Phys Chem 100:13148
23. Brunschwig BS, Creutz C, Sutin N (2002) Chem Soc Rev 31:168
24. Trautwein AX, Bill E, Bominaar EL, Winkler H (1991) Struct Bond 78:1
25. Demadis KD, Hartshorn CM, Meyer TJ (2001) Chem Rev 101:2655
26. Bersuker IB, Borshch SA (1992) Adv Chem Phys 81:703
27. Coropceanu VP, Prassides K (1988) Chem Phys Lett 289:53
28. Coropceanu VP, Meier C, Trautwein AX (2000) Chem Phys Lett 323:14
29. Coropceanu V, Brédas JL, Winkler H, Trautwein AX (2002) J Chem Phys 116:8152
30. Lahlil K, Moradpour A, Bowlas C, Menou F, Cassoux P, Bonvoisin J, Launay JP, Dive G, Dehareng D (1995) J Am Chem Soc 117:9995
31. Nelsen SF, Ismagilov R, Trieber DA (1997) Science 278:846
32. Lambert C, Nöll G (1999) J Am Chem Soc 121:8434
33. Lindeman SV, Rosokha SV, Sun D, Kochi JK (2002) J Am Chem Soc 124:843
34. Coropceanu V, Malagoli M, André JM, Brédas JL (2001) J Chem Phys 115:10409
35. Coropceanu V, Malagoli M, André JM, Brédas JL (2002) J Am Chem Soc 124:10519
36. Risko C, Barlow S, Coropceanu V, Halik M, Brédas JL, Marder SR (2003) Chem Commum 194
37. Malagoli M, Brédas JL (2000) Chem Phys Lett 327:13.
38. Lee C, Yang W, Parr RG (1988) Phys Rev B 37:785
39. Becke AD (1988) Phys Rev A 38:3098
40. Frisch MJ, et al (1998) Gaussian 98, revision A.9. Gaussian, Pittsburgh, PA
41. Coropceanu V, Malagoli M, da Silva Filho DA, Gruhn NE, Bill TG, Brédas JL, (2002) Phys Rev Lett 27:275503
42. Devos A, Lannoo M (1998) Phys Rev B 58:8236
43. Kato T, Yamabe T (2001) J Chem Phys 115:8592
44. Closs GL, Miller JR (1988) Science 240:440
45. Hupp JT, Williams RD (2001) Acc Chem Res 34:808
46. Kobori Y, Yago T, Akiyama K, Tero-Kubota S (2001) J Am Chem Soc 123:9722
47. Gruhn NE, da Silva Filho DA, Bill TG, Malagoli M, Coropceanu V, Kahn A, Brédas JL (2002) J Am Chem Soc 124:7918
48. Robin MB, Day P (1967) Adv Inorg Chem Radiochem 10:247
49. Piepho SB, Krausz ER, Schatz PN (1978) J Am Chem Soc 100:2996
50. Wong KY, Schatz PN (1981) Prog Inorg Chem 28:369
51. Root LJ, Ondrechen MJ (1982) Chem Phys Lett 93:421
52. Ondrechen MJ, Ko J, Zhang LT (1987) J Am Chem Soc 109:1672
53. Piepho SB (1988) J Am Chem Soc 110 6319
54. Piepho SB (1990) J Am Chem Soc 112: 4197
55. (a) Hush NS (1990) In: Brown DB (ed) Mixed-valence compounds: Theory and applications in chemistry, physics, geology and biology. Reidel, Dordrecht, p 151; (b) Reimers R, Hush NS (1996) Chem Phys 208:177
56. Cave RJ, Newton MD (1996) Chem Phys Lett 249:15
57. Casida ME, Jamorski C, Casida KC, Salahub DR (1998) J Chem Phys 108:4439; (b) Stratmann RE, Scuseria GE, Frisch MJ (1998) J Chem Phys 109:8218
58. Koopmans T (1933) Physica 1:104
59. Bally T, Borden WT (1999) Rev Comput Chem 13:1
60. Creutz C, Newton MD, Sutin NJ (1994) Photochem Photobiol A 82:47
61. Nelsen SF, Newton MD (2000) J Phys Chem A 104:10023
62. Johnson RC, Hupp JT (2001) J Am Chem Soc 123:2053
63. Creutz C, Taube H (1969) J Am Chem Soc 91:3988